Spatial dynamics of laser-induced fluorescence in an intense laser beam: experiment and theory in alkali metal atoms

M. Auzinsh,* A. Berzins, R. Ferber, F. Gahbauer, and U. Kalnins
Laser Centre, The University of Latvia, 19 Rainis Boulevard, LV-1586 Riga, Latvia
(Dated: October 27, 2015)

We have shown that it is possible to model accurately optical phenomena in intense laser fields by taking into account the intensity distribution over the laser beam. We developed a theoretical model that divided an intense laser beam into concentric regions, each with a Rabi frequency that corresponds to the intensity in that region, and solved a set of coupled optical Bloch equations for the density matrix in each region. Experimentally obtained magneto-optical resonance curves for the $F_g = 2 \longrightarrow F_e = 1$ transition of the D_1 line of ^{87}Rb agreed very well with the theoretical model up to a laser intensity of around 200 mW/cm^2 for a transition whose saturation intensity is around 4.5 mW/cm^2. We have studied the spatial dependence of the fluorescence intensity in an intense laser beam experimentally and theoretically. An experiment was conducted whereby a broad, intense pump laser excited the $F_g = 4 \longrightarrow F_e = 3$ transition of the D_2 line of cesium while a weak, narrow probe beam scanned the atoms within the pump beam and excited the D_1 line of cesium, whose fluorescence was recorded as a function of probe beam position. Experimentally obtained spatial profiles of the fluorescence intensity agreed qualitatively with the predictions of the model.

PACS numbers: 32.60.+i,32.80.Xx,32.10.Fn

arXiv:1510.07518v1 [physics.atom-ph] 26 Oct 2015

I. INTRODUCTION

Coherent radiation can polarize the angular momentum distribution of an ensemble of atoms in various ways, creating different polarization moments, which modifies the way these atoms will interact with radiation. Carefully prepared spin polarized atoms can make the absorption highly dependent on frequency (electromagnetically induced transparency [1]), causing large values of the dispersion, which, in turn, are useful for such interesting effects as slow light [2] and optical information storage [3]. Electric and magnetic fields, external or inherent in the radiation fields, may also influence the time evolution of the spin polarization and cause measurable changes in absorption or fluorescence intensity and/or polarization. These effects are the basis of many magnetometry schemes [4, 5], and must be taken into account in atomic clocks [6] and when searching for fundamental symmetry violations [7] or exotic physics such as an electric dipole moment of the electron [8]. Sufficiently strong laser radiation creates atomic polarization in excited as well as in the ground state [9] The polarization is destroyed when the Zeeman sublevel degeneracy is removed by a magnetic field. Since the ground state has a much longer lifetime, very narrow magneto-optical resonances can be created, which are related to the ground-state Hanle effect (see [10] for a review). Such resonances were first observed in cadmium in 1964 [11].

The theory of magneto-optical resonances has been understood for some time(see [7, 9, 12] for a review), and bright (opposite sign) resonances have also been observed and explained [13–15]; the challenge in describing experiments lies in choosing the effects to be included in the numerical calculations so as to find a balance between computation time and accuracy. The optical Bloch equations (OBEs) for the density matrix have been used as early as 1978 to model magneto-optical resonances [16]. In order to achieve greater accuracy, later efforts to model signals took into account effects such as Doppler broadening, the coherent properties of the laser radiation, and the mixing of magnetic sublevels in an external magnetic field to produce more and more accurate descriptions of experimental signals [17]. Analytical models can also achieve excellent descriptions of experimental signals at low laser powers in the regime of linear excitation where optical pumping plays a negligible role [18, 19]. In recent years, excellent agreement has been achieved by numerical calculations even when optical pumping plays a role. However, as soon as the laser radiation begins to saturate the absorption transition, the model's accuracy suffers. The explanation has been that at high radiation intensities, it is no longer possible to model the relaxation of atoms moving in and out of the beam with a single rate constant [17, 20]. Nevertheless, accurate numerical models of situations in an intense laser field are very desirable, because they could arise in a number of experimental situations. Therefore, we have set out to model magneto-optical effects in the presence of intense laser radiation by taking better account of the fact that an atom experiences different laser intensity values as it passes through a beam. In practice, we solve the rate equations for the Zeeman coherences for different regions of the laser beam with a value of the Rabi frequency that more closely approximates the real situation in that part of the beam. To save computing time, stationary solutions to the rate equations for Zeeman sublevels and coherences are sought

*Electronic address: Marcis.Auzins@lu.lv

for each region [21]. With this simplification to take into account the motion of atoms through the beam, we could now obtain accurate descriptions of experimental signals up to much higher intensities for reasonable computing times. Moreover, the model can be used to study the spatial distribution of the laser induced fluorescence within the laser beam. We performed such a study theoretically and experimentally using two overlapping lasers: one spatially broad, intense pump laser, and a weaker, tightly focused, spatically narrow probe laser. The qualitative agreement between experimental and theoretical fluorescence intensity profiles indicates that the model is a useful tool for studying fluorescence dynamics as well as for modelling magneto-optical signals at high laser intensities.

II. THEORY

The theoretical model used here is a further development of previous efforts [22], which has been subjected to some initial testing in the specialized context of an extremely thin cell [23]. The description of coherent processes starts with the optical Bloch equation (OBE):

$$i\hbar\frac{\partial\rho}{\partial t} = \left[\hat{H},\rho\right] + i\hbar\hat{R}\rho, \tag{1}$$

where ρ is the density matrix describing the atomic state, $\hat{H}$ is the Hamiltonian of the system, and $\hat{R}$ is an operator that describes relaxation. These equations are transformed into rate equations that are solved under stationary conditions in order to obtain the Zeeman coherences in the ground ($\rho_{g_i g_j}$) and excited ($\rho_{e_i e_j}$) states[21]. However, when the intensity distribution in the beam is not homogeneous, more accurate results can be achieved by dividing the laser beam into concentric regions and solving the OBEs for each region separately while accounting for atoms that move into and out of each region as they fly through the beam. Figure 1 illustrates the idea. The top part of the figure shows the intensity profile of the laser beam, while the bottom part of the figure shows a cross-section of the laser beam indicating the concentric regions.

In order to account for particles that leave one region and enter the next, an extra term must be added to the OBE:

$$-i\hbar\hat{\gamma}_t\rho + i\hbar\hat{\gamma}_t\rho'. \tag{2}$$

In this term, ρ' is the density matrix of the particles entering the region (identical to the density matrix of the previous region), and $\hat{\gamma}_t$ is an operator that accounts for transit relaxation. This operator is essentially a diagonal matrix with elements $\hat{\gamma}_{t_{ij}} = (v_{yz}/s_n)\delta_{ij}$, where v_{yz} characterizes the particle speed in the plane perpendicular to the beam and s_n is the linear dimension of the region. To simplify matters, we treat particle motion in only one direction and later average with particles that

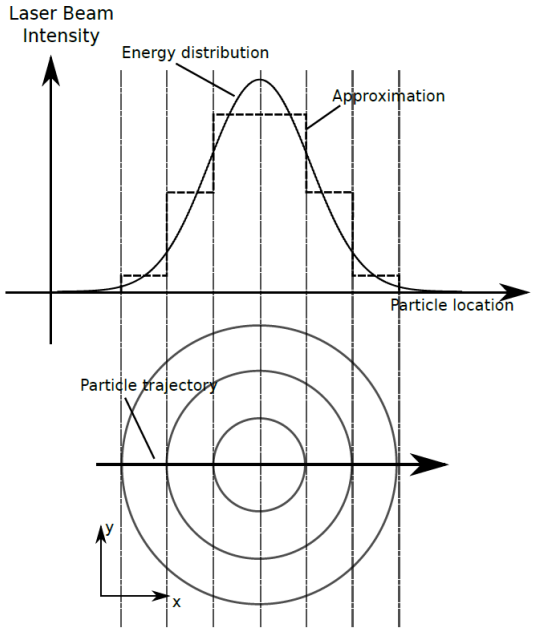

FIG. 1: Laser beam profile split into a number of concentric regions.

move in the other direction. In that case, $\rho' = \rho^{n-1}$. Thus, the rate equations for the density matrix ρ^n of the $n$textsuperscriptth region become

$$\begin{aligned} i\,\hbar\frac{\partial\rho^n}{\partial t} &= \left[\hat{H},\rho^n\right] + i\,\hbar\hat{R}\rho^n - i\,\hbar\hat{\gamma_t}^n\rho^n \\ &\quad + i\,\hbar\hat{\gamma_t}^n\rho^{n-1} - i\,\hbar\hat{\gamma_c}\rho^n + i\,\hbar\hat{\gamma_c}\rho^0. \end{aligned} \tag{3}$$

In this equation the relaxation operator $\hat{R}$ describes spontaneous relaxation only and $\hat{\gamma_c}$ is the collisional relaxation rate, which, however, becomes significant only at higher gas densities.

Next, the rotating wave approximation [24] is applied to the OBEs, which yield stochastic differential equations that can be simplified by means of the decorrelation approach [25]. Since the measurable quantity is merely light intensity, a formal statistical average is performed over the fluctuating phases of these stochastic equations, making use of the decorrelation approximation [21]. As a result, the density matrix elements that correspond to optical coherences are eliminated and one is left with rate

equations for the Zeeman coherences:

$$\begin{aligned}\frac{\partial\rho^n_{g_i,g_j}}{\partial t} &= \sum_{e_k,e_m}\left(\Xi^n_{g_ie_m}+(\Xi^n_{e_kg_j})^*\right)d^*_{g_ie_k}d_{e_mg_j}\rho^n_{e_ke_m}\\ &-\sum_{e_k,g_m}(\Xi^n_{e_kg_j})^*d^*_{g_ie_k}d_{e_kg_m}\rho^n_{g_mg_j}\\ &-\sum_{e_k,g_m}\Xi^n_{g_ie_k}d^*_{g_me_k}d_{e_kg_j}\rho^n_{g_ig_m}\\ &-i\omega_{g_ig_j}\rho^n_{g_ig_j}+\sum_{e_ke_l}\Gamma^{e_ke_l}_{g_ig_j}\rho^n_{e_ke_l}-\gamma_t\rho^n_{g_ig_j}\\ &+\gamma^n_t\rho^{n-1}_{g_ig_j}-\gamma^n_c\rho^n_{g_ig_j}+\gamma_c\rho^0_{g_ig_j}\end{aligned}\tag{4}$$

$$\begin{aligned}\frac{\partial\rho^n_{e_i,e_j}}{\partial t} &= \sum_{g_k,g_m}\left((\Xi^n_{e_ig_m})^*+\Xi^n_{g_ke_j}\right)d^*_{e_ig_k}d_{g_me_j}\rho^n_{g_kg_m}\\ &-\sum_{g_k,e_m}\Xi^n_{g_ke_j}d_{e_ig_k}d^*_{g_ke_m}\rho^n_{e_me_j}\\ &-\sum_{g_k,e_m}(\Xi^n_{e_ig_k})^*d_{e_mg_k}d^*_{g_ke_j}\rho^n_{e_ie_m}\\ &-i\omega_{e_ie_j}\rho^n_{e_ie_j}-\Gamma\rho^n_{e_ie_j}-\gamma^n_t\rho^n_{e_ie_j}\\ &+\gamma^n_t\rho^{n-1}_{e_ie_j}-\gamma_c\rho^n_{e_ie_j}.\end{aligned}\tag{5}$$

In both equations, the first term describes population increase and creation of coherence due to induced transitions, the second and third terms describe population loss due to induced transitions, the fourth term describes the destruction of Zeeman coherences due to the splitting $\omega g_i g_j$, respectively, $\omega_{e_ie_j}$ of the Zeeman sublevels in an external magnetic field, and the fifth term in Eq. 5 describes spontaneous decay with $\Gamma\rho^n_{e_ie_j}$ giving the spontaneous rate of decay for the excited state. At the same time the fifth term in Eq. 4 describes the transfer of population and coherences from the excited state matrix element $\rho_{e_ke_l}$ to the ground state density matrix element $\rho_{g_ig_j}$ with rate $\Gamma^{e_ke_l}_{g_ig_j}$. These transfer rates are related to the rate of spontaneous decay Γ for the excited state. Explicit expressions for these $\Gamma^{e_ke_i}_{g_ig_j}$ can be calculated from quantum angular momentum theory and are given in [9]. The remaining terms have been described previously in the context of Eqns. 2 and 3. The laser beam interaction is represented by the term

$$\Xi_{g_ie_j}=\frac{|\boldsymbol{\varepsilon}^n|^2}{\frac{\Gamma+\Delta\omega}{2}+i\left(\bar{\omega}-\mathbf{k}\cdot\mathbf{v}+\omega_{g_ie_j}\right)},\tag{6}$$

where $|\boldsymbol{\varepsilon}^n|^2$ is the laser field's electric field strength in the nth region, Γ is the spontaneous decay rate, $\Delta\omega$ is the laser beam's spectral width, $\bar{\omega}$ is the laser frequency, $k\cdot v$ gives the Doppler shift, and $\omega_{g_ie_j}$ is the difference in energy between levels g_i and e_j. The system of linear equations can be solved for stationary conditions to obtain the density matrix ρ.

From the density matrix one can obtain the fluorescence intensity from each region for each velocity group v and given polarization $\boldsymbol{\varepsilon}_f$ up to a constant factor of $\tilde{I}_0$ [26–28]:

$$I_n(v,\boldsymbol{\varepsilon}_f)=\tilde{I}_0\sum_{g_i,e_j,e_k}d^{*(ob)}_{g_ie_j}d^{(ob)}_{e_kg_i}\rho_{e_je_k}.\tag{7}$$

From these quantities one can calculate the total fluorescence intensity for a given polarization $\boldsymbol{\varepsilon}_f$:

$$I(\boldsymbol{\varepsilon}_f)=\sum_n\sum_v f(v)\Delta v\frac{A_n}{A}I_n(v,\boldsymbol{\varepsilon}_f).\tag{8}$$

Here the sum over n represents the sum over the different beam regions of relative area A_n/A as they are traversed by the particle, v is the particle velocity along the laser beam, and $f(v)\Delta v$ gives the number of atoms with velocity $v\pm\Delta v/2$.

In practice, we do not measure the electric field strength of the laser field, but the intensity $I=P/A$, where P is the laser power and A is the cross-sectional area of the beam. In the theoretical model it is more convenient to use the Rabi frequency Ω_R, here defined as follows:

$$\Omega_R=k_R\frac{||d||\cdot||\epsilon||}{\hbar}=k_R\frac{||d||}{\hbar}\sqrt{\frac{2I}{\epsilon_0 nc}},\tag{9}$$

where $||d||$ is the reduced dipole matrix element for the transition in question, ϵ_0 is the vacuum permittivity, n is the index of refraction of the medium, c is the speed of light, and k_R is a factor that would be unity in an ideal case, but is adjusted to achieve the best fit between theory and experiment since the experimental situation will always deviate from the ideal case in some way. We assume that the laser beam's intensity distribution follows a Gaussian distribution. We define the average value of Ω_R for the whole beam by taking the weighted average of a Gaussian distribution on the range [0,FWHM/2], where FWHM is the full width at half maximum. Thus it follows that the Rabi frequency at the peak of the intensity distribution (see Fig. 1) is $\Omega_R=0.721\Omega_{peak}$. From there the Rabi frequency of each region can be obtained by scaling by the value of the Gaussian distribution function.

III. EXPERIMENTAL SETUP

The theoretical model was tested with two experiments. The first experiment measured magneto-optical resonances on the D_1 line of ^{87}Rb and is shown schematically in Fig. 2. The experiment has been described elsewhere along with comparison to an earlier version of the theoretical model that did not divide the laser beam into separate regions [29]. The laser was an extended cavity diode laser, whose frequency could be scanned by applying a voltage to a piezo crystal attached to the grating. Neutral density (ND) filters were used to regulate the laser intensity, and linear polarization was obtained using a Glan-Thomson polarizer. A set of three orthogonal Helmholtz coils scanned the magnetic field along

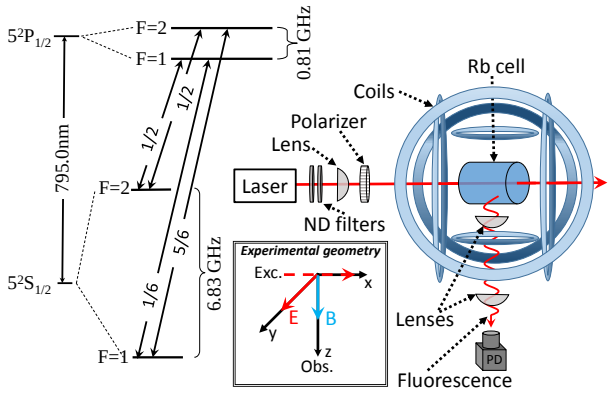

FIG. 2: (Color online) Basic experimental setup for measuring magneto-optical resonances. The inset on the left shows the level diagram of ^{87}Rb [30]. The other inset shows the geometrical orientation of the electric field vector E, the magnetic field vector B, and laser propagation direction (Exc.) and observation direction (Obs.).

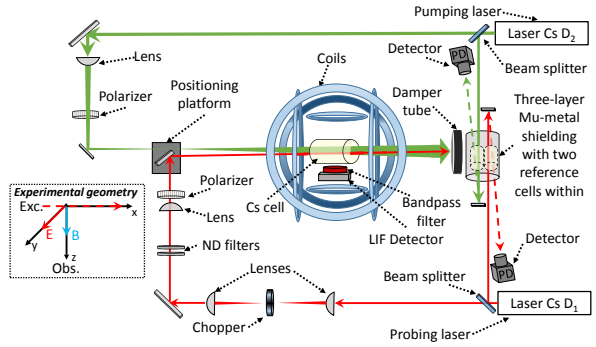

FIG. 3: (Color online) Experimental setup for the two-laser experiment. The lasers were stabilized by two Toptica Digilok modules locked to error signals generated from saturated absorption spectroscopy measurements made in a separate, magnetically shielded cell.

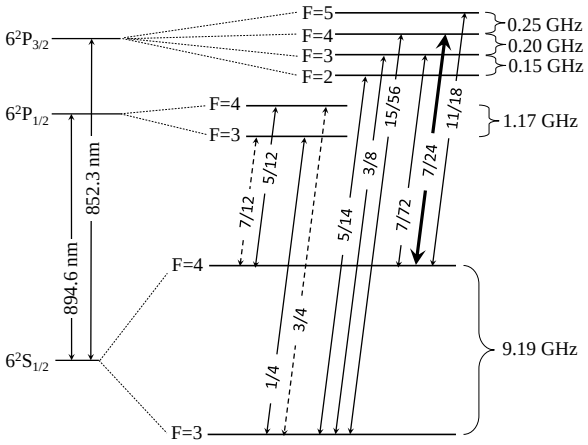

FIG. 4: Level scheme for the two-laser experiment. The bold, solid arrow represents the pump laser transition, whereas the arrows with dashed lines represent the scanning laser transitions. Other transitions are given as thin, solid lines.

the z axis while compensating the ambient field in the other directions. A pyrex cell with a natural isotopic mixture of rubidium at room temperature was located at the center of the coils. The total laser induced fluorescence (LIF) in a selected direction (without frequency or polarization selection) was detected with a photodiode (Thorlabs FDS-100) and data were acquired with a data acquisition card (National Instruments 6024E) or a digital oscilloscope (Agilent DSO5014). To generate the magnetic field scan with a rate of about 1 Hz, a computer-controlled analog signal was applied to a bipolar power supply (Kepco BOP-50-8M). The laser frequency was simultaneously scanned at a rate of about 10-20 MHz/s, and it was measured by a wavemeter (HighFinnesse WS-7). The laser beam was characterized using a beam profiler (Thorlabs BP104-VIS).

A second experimental setup was used to study the spatial profile of the fluorescence generated by atoms in a laser beam at resonance. It is shown in Fig. 3. Here two lasers were used to excite the D_1 and D_2 transitions of cesium. Both lasers were based on distributed feedback diodes from toptica (DL100-DFB). One of the lasers (Cs D_2) served as a pump laser with a spatially broad and intense beam, while the other (Cs D_1), spatially narrower beam probed the fluorescence dynamics within the pump beam. Figure 4 shows the level scheme of the excited transitions. Both lasers were stabilized with saturation absorption signals from cells shielded by three layers of mu-metal. Mu-metal shields were used to avoid frequency drifts due to the magnetic field scan performed in the experiment and other magnetic field fluctuations in the laboratory.

A bandpass filter (890 nm $\pm$ 10 nm) was placed before the photodiode. To reduce noise from the intense pump beam, the probe beam was modulated by placing a mechanical chopper near its focus, and the fluorescence signal was passed through a lock-in amplifier and recorded on a digital oscilloscope (Yokogawa DL-6154). The probe laser was scanned through the pump laser beam profile using a mirror mounted on a moving platform (Nanomax MAX301 from Thorlabs) with a scan range of 8 mm in one dimension. The probing beam itself had a full width at half maximum (FWHM) diameter of 200 µm with typical laser power of 100 µW. The pump beam width was 1.3 mm (FWHM) and its power was 40 mW. This laser beam diameter was achieved by letting the laser beam slowly diverge after passing the focal point of a lens with focal length of 1 m. The pump laser beam diverged slowly enough to be effectively constant within the vapor cell. The probe beam was also focussed by the same lens to reach its focus point inside

the cell.

IV. APPLICATION OF THE MODEL TO MAGNETO-OPTICAL SIGNALS OBTAINED FOR HIGH LASER POWER DENSITIES

As a first test for the numerical model with multiple regions inside the laser beam, we used the model to calculate the shapes of magneto-optical resonances for ^{87}Rb in an optical cell. The experimental setup was described earlier (see Fig. 2). Figure 5(a)–(c) show experimental signals (markers) and theoretical calculations (curves) of magneto-optical signals in the $F_g = 2 \longrightarrow F_e = 1$ transition of the D_1 line of ^{87}Rb. Three theoretical curves are shown: curve N1 was calculated assuming a laser beam with a single average intensity; curve N20 was calculated using a laser beam divided into 20 concentric regions; curve N20MT was calculated in the same way as curve N20, but furthermore the results were averaged also over trajectories that did not pass through the center. At the relatively low Rabi frequency of $\Omega_R = 2.5$ MHz [Fig. 5(a)] all calculated curves practically coincided and described well the experimental signals. The single region model treats the beam as a cylindrical beam with an intensity of 2 mW/cm^2, which is below the saturation intensity for that transition of 4.5 mW/cm^2 [30]. When the laser intensity was 20 mW/cm^2 ($\Omega_R = 8.0$ MHz), well above the saturation intensity, model N1 is no longer adequate for describing the experimental signals and model N20MT works slightly better [Fig. 5(b)]. In particular, the resonance becomes sharper and sharper as the intensity increases, and models N20 and N20MT reproduce this sharpness. Even at an intensity around 200 mW/cm^2 ($\Omega_R = 25$ MHz), the models with 20 regions describe the shape of the experimental curve quite well, while model N1 describes the experimental results poorly in terms of width and overall shape [Fig. 5(c)].

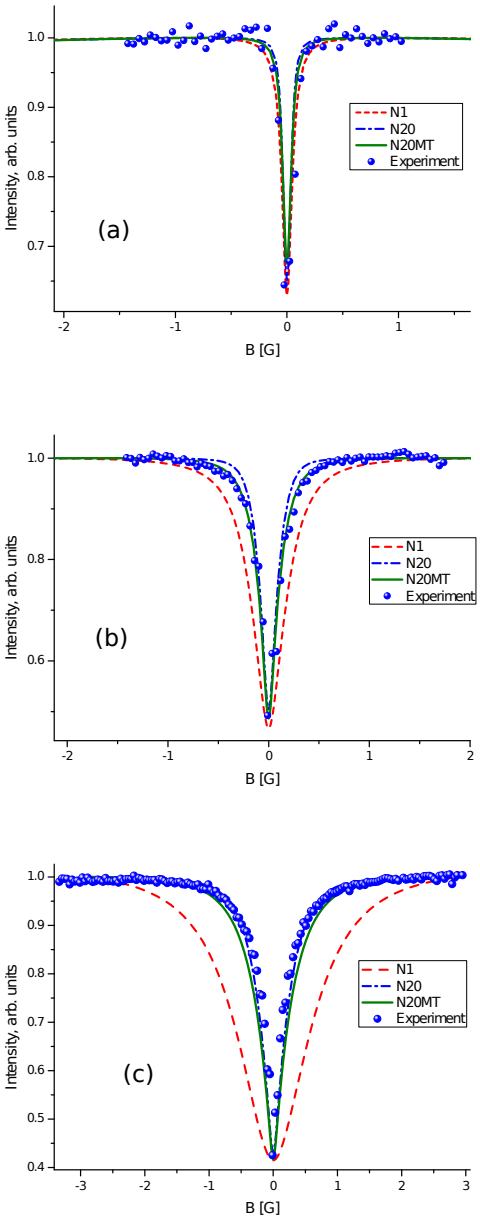

FIG. 5: (Color online) Magneto-optical resonances for the $F_g = 2 \longrightarrow F_e = 1$ transition of the D_1 line of ^{87}Rb. Filled circles represent experimental measurements for (a) 28 μW (Ω_R=2.5 MHz) (b) 280 μW (Ω_R=8.0 MHz), and (c) 2800 μW (Ω_R=25 MHz). Curve N1 (dashed) shows the results of a theoretical model that uses one Rabi frequency to model the entire beam profile. Curve N20 (dash-dotted) shows the result of the calculation when the laser beam profile is divided into 20 concentric circles, and the optical Bloch equations are solved separately for each circle. Curve N20MT (solid) shows the results for a calculation with 20 concentric regions when trajectories are taken into account that do not pass through the center of the beam.

V. INVESTIGATION OF THE SPATIAL DISTRIBUTION OF FLUORESCENCE IN AN INTENSE LASER BEAM

A. Theoretical investigation of the spatial dynamics of fluorescence in an extended beam

In order to describe the magneto-optical signals in the previous sections, the fluorescence from all concentric beam regions in models N20 and N20MT was summed, since usually experiments measure only total fluorescence (or absorption), especially if the beams are narrow. However, solving the optical Bloch equations separately for different concentric regions of the laser beam, it is possible to calculate the strength of the fluorescence as a function of distance from the center of the beam. With an appropriate experimental technique, the distribution

of fluorescence within a laser beam could also be measured.

Figure 6 shows the calculated fluorescence distribution as a function of position in the laser beam. As atoms move through the beam in one direction, the intense laser radiation optically pumps the ground state. In a very intense beam, the ground state levels that can absorb light have emptied even before the atoms reach the center (solid, green curve). Since atoms are actually traversing the beam from all directions, the result is a fluorescence profile with a reduction in intensity near the center of the beam (dashed, red curve). The effect of increasing the

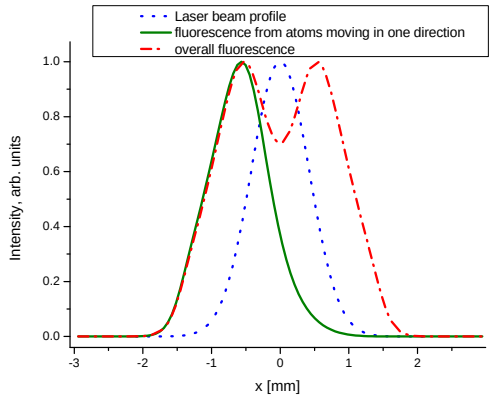

FIG. 6: (Color online) Fluorescence distribution as a function of position in the laser beam. Dotted (blue) line—laser beam profile, solid (green) line—fluorescence from atoms moving in one direction; dash-dotted (red) line—the overall fluorescence as a function of position that results from averaging all beam trajectories. Results from theoretical calculations.

laser beam intensity (or Rabi frequency) can be seen in Fig. 7. At a Rabi frequency of $\Omega_R = 0.6$ MHz, the fluorescence profile tracks the intensity profile of the laser beam exactly. When the Rabi frequency is increased ten times ($\Omega_R = 6.0$ MHz), which corresponds to an intensity increase of 100, the fluorescence profile already appears somewhat deformed and wider than the actual laser beam profile. At Rabi frequencies of $\Omega_R = 48.0$ MHz and greater, the fluorescence intensity at the center of the intense laser beam is weaker than towards the edges as a result of the ground state being depleted by the intense radiation before the atoms reach the center of the laser beam.

B. Experimental study of the spatial dynamics of excitation and fluorescence in an intense, extended beam

In order to test our theoretical model of the spatial distribution of fluorescence from atoms in an intense, extended pumping beam, we decided to record magneto-optical resonances from various positions in the pumping beam. The experimental setup is shown in Fig. 3. To

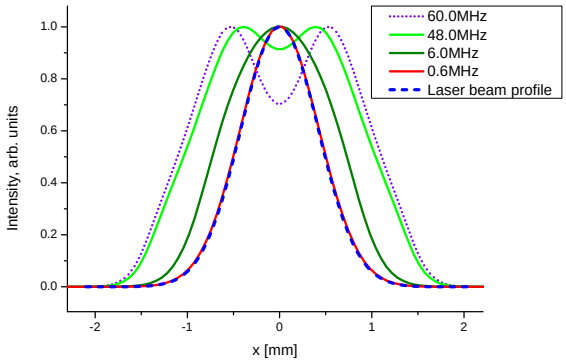

FIG. 7: (Color online) Fluorescence distribution as a function of position in the laser beam for various values of the Rabi frequency. Results from theoretical calculations. As the Rabi frequency increases, the distribution becomes broader.

visualize these data, surface plots were generated where one horizontal axis represented the magnetic field and the other, the position of the probe beam relative to the pump beam axis. The height of the surface represented the fluorescence intensity. In essense, the surface consists of a series of magneto-optical resonances recorded for a series of positions of the probe beam axis relative the the pump beam axis. Fig. 8 shows the results for experiments [(a)] and calculations [(b)] for which the pump beam was tuned to the $F_g = 4 \longrightarrow F_e = 4$ transition of the Cs D_2 line and the probe beam was tuned to the $F_g = 4 \longrightarrow F_e = 3$ transition of the Cs D_1 line. One can see that the theoretical plot reproduces qualitatively all the features of the experimental measurement. Similar agreement can be observed when the probe beam was tuned to the $F_g = 3 \longrightarrow F_e = 4$ transition of the Cs D_1 line, as shown in Fig. 9.

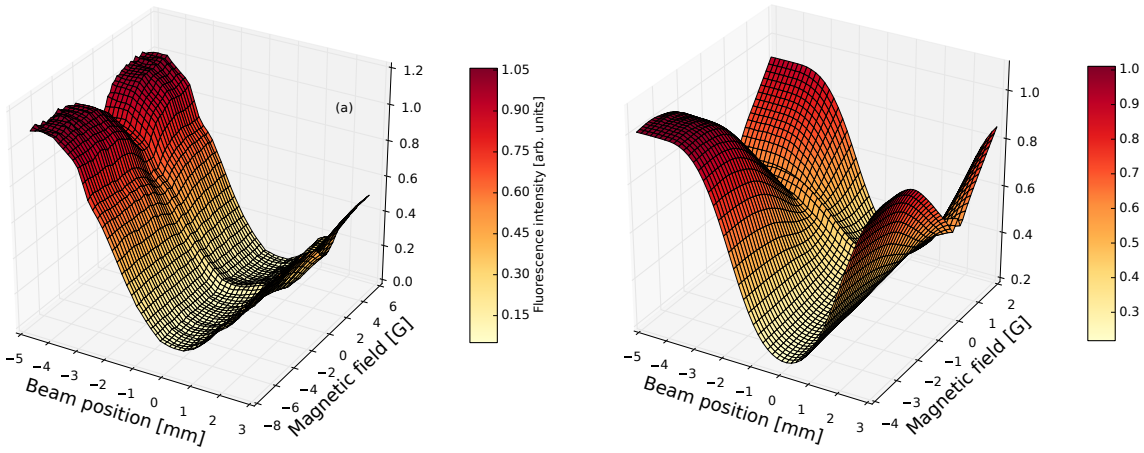

FIG. 8: (Color online) Magneto-optical resonances produced for various positions of the probing laser beam ($F_g = 4 \longrightarrow F_e = 3$ transition of the D_1 line of cesium) with respect to the pump laser beam ($F_g = 4 \longrightarrow F_e = 4$ transition of the D_2 line of cesium): (a) experimental results and (b) theoretical calculations.

VI. CONCLUSIONS

We have set out to model magneto-optical signals more accurately at laser intensities significantly higher than the saturation intensity by dividing the laser beam into concentric circular regions and solving the rate equations for Zeeman coherences in each region while taking into account the actual laser intensity in that region and the transport of atoms between regions. This approach was used to model magneto-optical resonances for the $F_g = 2 \longrightarrow F_e = 1$ transitions of the D_1 line of ^{87}Rb, comparing the calculated curves to measured signals. We have demonstrated that good agreement between theory and experiment can be achieved up to Rabi frequencies of at least 25 MHz, which corresponds to a laser intensity of 200 mW/cm^2, or more than 40 times the saturation intensity of the transition. As an additional check on the model, we have studied the spatial distribution of the fluorescence intensity within a laser beam theoretically and experimentally. The results indicated that at high laser power densities, the maximum fluorescence intensity is not produced in the center of the beam, because the atoms have been pumped free of absorbing levels prior to reaching the center. We compared experimental and theoretical signals of magneto-optical resonance signals obtained by exciting cesium atoms with a narrow, weak probe beam tuned to the D_1 transition at various locations inside a region illuminated by an intense pump beam tuned to the D_2 transition and obtained good qualitative agreement.

Acknowledgments

We gratefully acknowledge support from the Latvian Science Council Grant Nr. 119/2012 and from the University of Latvia Academic Development Project Nr. AAP2015/B013.

[1] S. E. Harris, J. E. Field, and A. Imamoglu, Physical Review Letters **64**, 1107 (1990).
[2] L. V. Hau, S. E. Harris, Z. Dutton, and C. H. Behroozi, Nature **397**, 594 (1999).
[3] C. Liu, Z. Dutton, C. H. Behroozi, and L. V. Hau, Nature **409**, 490 (2001).
[4] M. O. Scully and M. Fleischhauer, Phys. Rev. Lett. **69**, 1360 (1992).
[5] D. Budker and M. V. Romalis, Nature Physics **3**, 227 (2007).
[6] S. Knappe, P. D. D. Schwindt, V. Shah, L. Hollberg, J. Kitching, L. Liew, and J. Moreland, Opt. Express **13**, 1249 (2005).
[7] D. Budker, W. Gawlik, D. F. Kimball, S. M. Rochester, V. V. Yashchuk, and A. Weis, Reviews of Modern Physics **74**, 1153 (2002), ISSN 15390756.
[8] B. Regan, E. D. Commins, C. J. Schmidt, and D. DeMille, Phys. Rev. Lett. **88**, 071805 (2002), URL `http://journals.aps.org/prl/abstract/10.1103/PhysRevLett.88.071805`.
[9] M. Auzinsh, D. Budker, and S. M. Rochester, *Optically Polarized Atoms* (Oxford University Press, Great Cardendon Street, 2010), ISBN 978-0-19-956512-2.
[10] E. Arimondo (Elsevier, 1996), vol. 35 of *Elsevier Science B.V.*, p. 259, ISBN 978-0-444-82309-0.
[11] J. C. Lehmann and C. Cohen-Tannoudji, C.R. Acad. Sci. (Paris) **258**, 4463 (1964).
[12] E. B. Alexandrov, M. Auzinsh, D. Budker, D. F. Kimball, S. Rochester, and V. V. Yashchuk, J. Opt. Soc. Am. B **22**, 7 (2005).

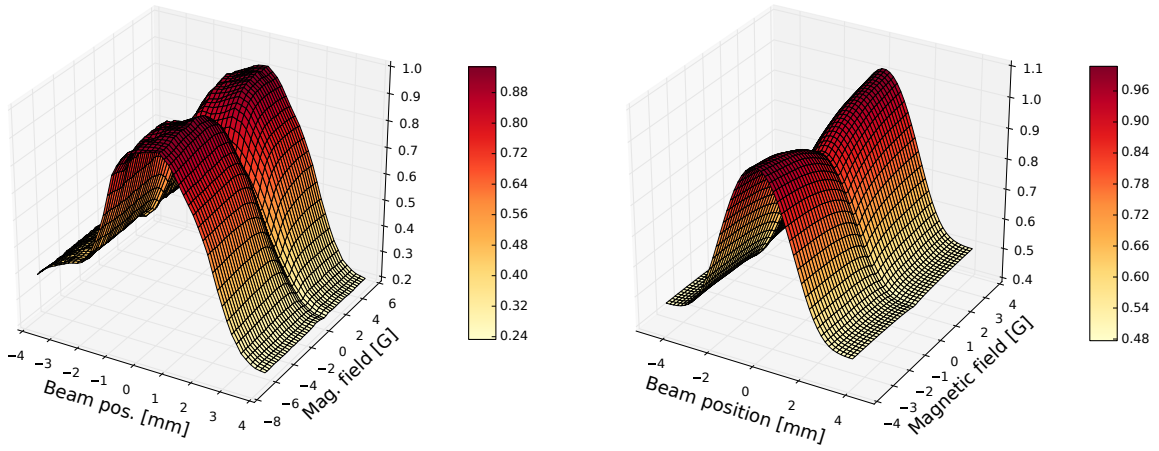

FIG. 9: (Color online) Magneto-optical resonances produced for various positions of the probe laser beam ($F_g = 3 \longrightarrow F_e = 4$ transition of the D_1 line of cesium) with respect to the pump laser beam ($F_g = 4 \longrightarrow F_e = 4$ transition of the D_2 line of cesium): (a) experimental results and (b) theoretical calculations.

[13] A. P. Kazantsev, V. S. Smirnov, A. M. Tumaikin, and I. A. Yagofarov, Opt. Spectrosk. (USSR) **57**, 116 (1984).

[14] F. Renzoni, S. Cartaleva, G. Alzetta, and E. Arimondo, Physical Review A **63**, 065401 (2001).

[15] J. Alnis and M. Auzinsh, Physical Review A **63**, 023407 (2001), arXiv:physics/0011050.

[16] J. L. Picqué, J. Phys. B: Atom. Molec. Phys. **11**, L59 (1978).

[17] M. Auzinsh, R. Ferber, F. Gahbauer, A. Jarmola, and L. Kalvans, Physical Review A **78**, 013417 (2008), ISSN 10941622.

[18] N. Castagna and A. Weis, Phys. Rev. A **84**, 053421 (2011).

[19] E. Breschi and A. Weis, Physical Review A **86**, 053427 (2012).

[20] M. P. Auzinsh, R. S. Ferber, and I. Y. Pirags, Journal of Physics B: Atomic and Molecular Physics **16**, 2759 (1983).

[21] K. Blushs and M. Auzinsh, Physical Review A **69**, 063806 (2004).

[22] M. Auzinsh, A. Berzins, R. Ferber, F. Gahbauer, L. Kalvans, A. Mozers, and A. Spiss, Physical Review A **87**, 033412 (2013), URL `http://link.aps.org/doi/10.1103/PhysRevA.87.033412`.

[23] M. Auzinsh, A. Berzins, R. Ferber, F. Gahbauer, U. Kalnins, L. Kalvans, R. Rundans, and D. Sarkisyan, Phys. Rev. A **91**, 023410 (2015).

[24] L. Allen and J. H. Eberly, *Optical Resonance and Two Level Atoms* (Wiley, New York, 1975).

[25] N. G. van Kampen, Physics Reports **24**, 171 (1976).

[26] M. Auzinsh and R. Ferber, *Optical Polarization of Molecules* (Cambridge University Press, 2005), ISBN 978-0-521-44346-3.

[27] J. P. Barrat and C. Cohen-Tannoudji, J. Phys. Radium **22**, 443 (1961).

[28] M. I. Dyakonov, Sov. Phys. JETP **200**, 1484 (1965).

[29] M. Auzinsh, R. Ferber, F. Gahbauer, A. Jarmola, and L. Kalvans, Physical Review A **79**, 053404 (2009), ISSN 10941622.

[30] D. A. Steck, *Rubidium 87 D Line Data* (2009), revision 2.1.2, 12 August 2009, URL `http://steck.us/alkalidata`.